# Viscoelastic Properties of Clay-Containing Nanocomposites of Thermotropic Liquid-Crystal Polymer

Jayita Bandyopadhyay, Suprakas Sinha Ray,* Mosto Bousmina*

The nanocomposites of liquid-crystal polymer (LCP) with two different weight per cents of clay were prepared *via* the melt extrusion method. To investigate the properties of the materials in the linear and non-linear viscoelastic regions, both oscillatory and rotational tests were carried out. The results showed that the nanocomposite with higher clay content exhibited an almost defectless partially cross-linked structure compared to the nanocomposite with lower clay content or the pure LCP. The linear stress relaxation measurements revealed that the pure LCP relaxed faster than nanocomposites after imposition of a constant strain for a specific time. During the step rate relaxation test, high shear rate modified the defects in the pure LCP very quickly and probably attained almost an equilibrium position while the nanocomposite samples showed strong shear thinning behaviour.
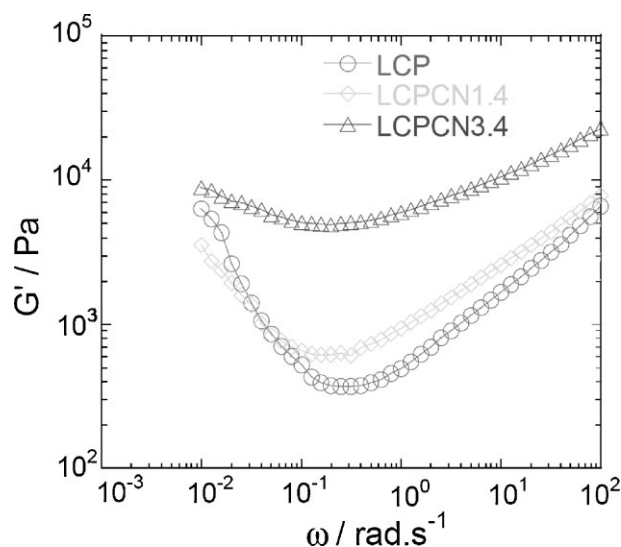
Introduction

Over the past few years, clay-containing polymer nanocomposites have attracted considerable attention from the perspectives of both fundamental research and real applications.[1] To date, almost all polymer matrices have been used for the preparation of nanocomposites with either pristine or organically modified clays [1–13]; however, there are only a few reports on the clay-containing nanocomposites based on liquid-crystal polymers (LCPs).[14–20] LCPs are well known for their excellent properties such as high strength and stiffness, low melt viscosity and high chemical and thermal resistance.[21,22] In our recent article,[23] we reported, for the first time, how the structure of the LCP changes after the preparation of the nanocomposites with organoclay and how the clay particles affect the properties of the LCP. Nanocomposites containing two different weight percents of dimethyl dihydrogenated-tallow quaternary ammonium-modified montmorillonite (MMT) (commercially known as C20A) were prepared *via* the melt extrusion method using a twin-screw extruder.[23] Wide-angle X-ray diffraction (WAXD) patterns and transmission electron microscopy studies

J. Bandyopadhyay, S. Sinha Ray, M. Bousmina
Department of Chemical Engineering Laval University, Quebec, Canada G1K 7P4
J. Bandyopadhyay, S. Sinha Ray
National Centre for Nano-Structured Materials, Council for Scientific and Industrial Research, Pretoria 0001, Republic of South Africa
E-mails: rsuprakas@csir.co.za; bousmina@gch.ulaval.com

showed the formation of intercalated nanocomposites. The two-dimensional (2-D) X-ray diffraction (XRD) patterns in both the small and wide-angle regions revealed that very little smectic-like ordering was present in the pure LCP, whereas in the nanocomposites, the polymer chains not only oriented in the direction of the dispersed clay layers, but also the ordering in alignment was also improved.[23]

The main objective of this work is to understand the effect of the addition of C20A organoclay on the melt-state rheological behaviour of LCP. Melt-state rheological behaviour can provide a good understanding of processing and structural characterisation of polymer composite materials. The rheological properties of polymer-filled composite systems are strongly influenced by the dispersion characteristics of the filler particles in the polymer matrix, which actually depends on the interfacial interactions between the filler surface and polymer matrix and the flow history.[24–29] In the case of LCP, the rheological properties are very sensitive to phase changes. Therefore, rheology will potentially offer a means to study the effect of the addition of organoclay on the phase changes of LCP in the melt-state.

Pure LCP and nanocomposites were examined under both dynamic oscillatory and rotational motions using a strain-controlled rheometer. All experiments were conducted in the molten state at a temperature of 290 °C under a nitrogen atmosphere using parallel plate geometry.

Experimental Part

Materials and Nanocomposite Preparation

The commercially available main chain thermotropic LCP, Vectra B950 used in this study was supplied by Ticona (USA). Figure 1 represents the chemical formula of Vectra B950.

Dimethyl dehydrogenated tallow quaternary ammonium-modified MMT (commercially known as C20A, Southern Clay Products, USA) was used for the preparation of nanocomposites. Nanocomposites with two different loadings of C20A were prepared by melt-extrusion in a Haake twin-screw extruder at a screw speed of 30 rpm. The barrel temperatures used were 260, 270 and 270 °C, and the temperature of the capillary die was 270 °C. The samples (with thickness ≈1.2 mm) were moulded using a Carver laboratory press at 300 °C, under 2 MPa pressure for 2 min.

The amount of the inorganic part present in the nanocomposite samples was determined using a thermogravimetric analyser (TGA, Q500 TA Instrument). According to TGA data (conducted under air), the amount of the inorganic part present in the first batch of nanocomposite sample was 1.4% and that in the second batch of nanocomposite sample was 3.4%; hence, the abbreviations used for these nanocomposites were LCPCN1.4 and LCPCN3.4, respectively. The thermal stability of C20A at the processing conditions was also measured by TGA. Details can be found elsewhere.[23]

Rheological Property Measurements

The rheological properties of pure LCP and nanocomposite samples were measured in an ARES-LS strain controlled rheometer (Rheometric Scientific), using 25 mm diameter parallel plates, under a nitrogen environment at 290 °C. Six different types of tests were conducted: (i) the strain sweep at frequency, $\omega = 6.28$ rad · s^{-1} for strain, $\gamma = 0.006$–100%; (ii) the frequency sweep at $\gamma = 1\%$ within the ω range from 0.01 to 100 rad · s^{-1}; (iii) the temperature sweep at $\omega = 6.28$ rad · s^{-1} and $\gamma = 1\%$ for temperature = 290–350 °C with a temperature ramp of 5 °C · min^{-1}; (iv) stress relaxation at $\omega = 6.28$ rad · s^{-1} and applied $\gamma = 1\%$ for time = 500 s; (v) step rate test by increasing shear rate step by step from $0.01 \rightarrow 0.1 \rightarrow 0.5$ s^{-1} with time and then back to the initial shear rate of 0.01 s^{-1}; (vi) step rate relaxation test after imposition of a high shear rate (0.5 s^{-1}) for 1 000 s.

Small and Wide-Angle X-Ray Scattering (SWAXS) Measurements

In order to determine the structural modification–i.e. the phase change during the oscillatory tests at small amplitude–SWAXS experiments were performed using an Anton Paar SAXSess instrument, operated at 40 kV and 50 mA. The radiation used was a Ni filtered CuKα radiation source of wavelength (λ) 0.154 nm (PAN Analytical). Intensity profiles were obtained with a slit collimated compact Krathy Camera and recorded with a two-dimensional imaging plate. Sample to detector distance was 264.5 mm and covers the length of the scattering vector (q) from 0.1 to 28 nm^{-1}. Very thin sheets (≈90 µm) of samples were prepared by hot press-compression moulding of dried samples of LCP and nanocomposites at 290 °C under 2 metric ton pressures for 2 min. The total moulding time was 12 min. The samples were heated in a paste cell from room temperature to 280 °C and then cooled down to room temperature by a TCU50 (Anton-Paar) temperature-control unit, which is attached to the SAXSess instrument. SAXS data are collected at temperature of 280 °C. The samples were kept at this temperature for 5 min including 1 min exposure time under X-ray.

Results and Discussions

Oscillatory Tests

The oscillatory tests are important to analyse a material in the LVE region.
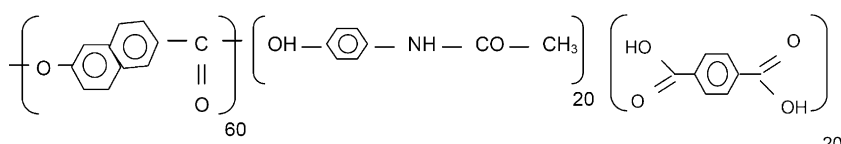
Figure 1. Molecular structure of Vectra B950.

Amplitude Sweep

To determine the effect of the incorporation of C20A on the structural modification of pure LCP with varying strain amplitude, strain sweep tests of pure LCP and nanocomposites containing two different loadings of MMT were carried out. Parts a–c of Figure 2 shows the storage modulus (G'), loss modulus (G''), and tan δ as a function of shear strain $\gamma = 0.006$–100% at $\omega = 6.28$ rad·s^{-1} and temperature $= 290\,°C$, for pure LCP, LCPCN1.4 and LCPCN3.4. Depending on the thermal expansion and dispersion of clay platelets at the experimental temperature, the normal force (NF) at the starting point of the experiment varied from sample to sample. From Figure 2, we see that for both LCP and LCPCN3.4 samples, in the LVE region, the elastic behaviour is dominant over the viscous one ($G' > G''$). Such a result indicates the formation of a gel structure for these two samples. Even if this is a weak gel structure, the samples exhibit a certain form-stability. On the other hand, in the case of the LCPCN1.4 sample, the value of G' is almost equivalent to the value of G''. This behaviour, sometimes called 'at the gel point' behaviour, indicates that the material is at the borderline between gel (solid) and sol (liquid) structures under this experimental condition.[30] At this particular frequency of oscillation, the structures of LCPCN1.4 are more flexible compared to those of the LCPCN3.4 and LCP samples. The yield values of the LVE plateau (γ_L) of various samples are given in Table 1. γ_L Represents a strain limit up to which one can consider no significant modification in the internal structure is taking place. The decreasing trend of γ_L with increase in clay content refers to the range of reversible viscoelastic behaviour is decreasing in LCPCNs. After the LVE range, the crossover point of $G' = G''$ is another yield point known as the flow point (γ_F) and the region between γ_L and γ_F is known as the yield zone. Table 1 shows a decrease in γ_F values for LCPCNs when compared to pure LCP. Again, the lowest γ_F value is observed for LCPCN1.4 as it is almost at the gel point. The amplitude sweep results do not simulate the material behaviour at rest. In order to evaluate a material at rest, it is essential to perform a frequency sweep test with strain amplitude in the LVE region (where any structural change is reversible). For this reason, the strain chosen for the frequency sweep tests is 1%.

Frequency Sweep Test

The frequency sweep experiment was carried out in a dynamic oscillation mode with a constant oscillation amplitude of 1% at an experimental temperature of 290 °C, and the results are summarised in Figure 3 and 4. In the low frequency region, after a certain frequency both moduli of LCP are showing uplifting nature with dominant
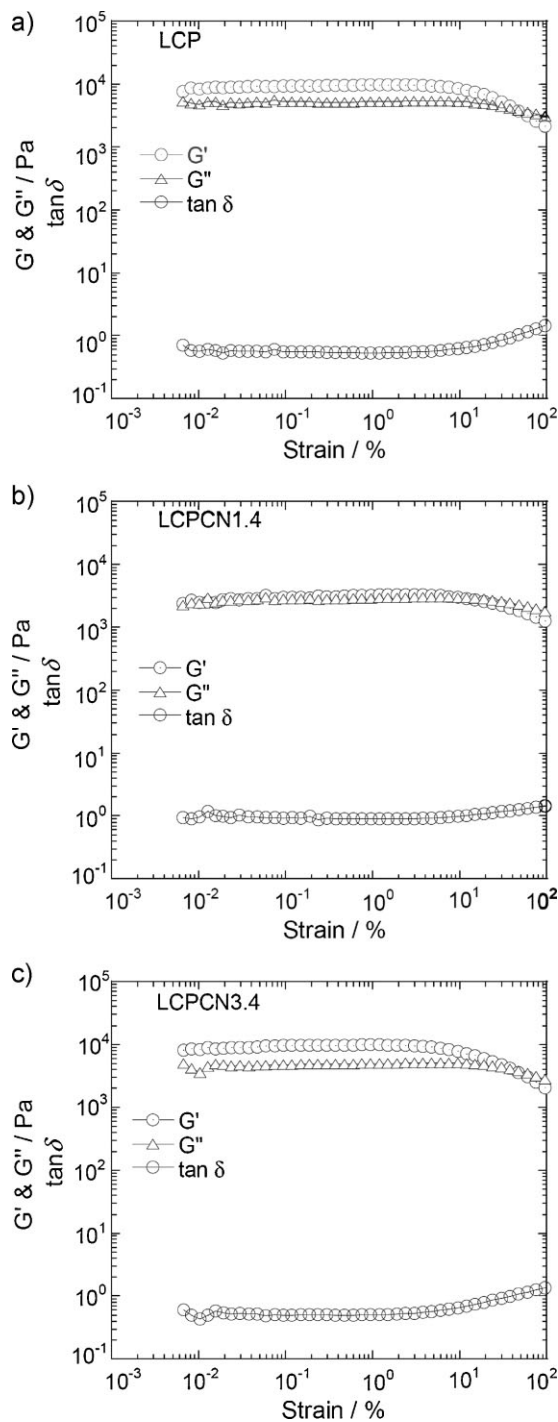

Figure 2. Strain amplitude sweep of LCP and LCPCNs at frequency $= 6.28$ rad·s^{-1} and temperature $= 290\,°C$ under nitrogen environment: (a) pure LCP, (b) LCPCN1.4 and (c) LCPCN3.4.

elastic behaviour (Figure 3a). In the case of LCPCN1.4, both moduli are also showing the same trend-like LCP; however, in the high frequency region the viscous property becomes less dominant over elastic property compared to pure LCP. With further increase in clay content, as in the case of

Table 1. Determination of LVE range of various samples.

Sample	γ_L	γ_F
	%	%
LCP	4.95	49.48
LCPCN1.4	4.79	15.15
LCPCN3.4	3.83	47.92

LCPCN3.4, results $G' > G''$ in the whole range of frequency examined with the uplifting nature of moduli in the low frequency region. However, it is very interesting to note that, the uplifting nature of both moduli becomes less prominent as clay loading increases. Another interesting observation is that the frequency at which both moduli starts to increase gradually shifts towards lower frequency region with increase in clay content.

In the presence of a small amount of layered silicate particles (as in the case of LCPCN1.4) because of intercalation the polymer chains are somehow restricted to flow. Thus, the dominating nature of G'' over G' becomes less pronounced in the high frequency region as observed in Figure 3b. With further increase in clay loading, for LCPCN3.4, the elastic behaviour is dominating over the viscous behaviour ($G' > G''$) in the whole frequency range examined (see Figure 3c). This is due to the presence of high cross-linking (physical–chemical network) along with the mechanical interaction (entanglements). The increase in cross-linking from LCPCN1.4 to LCPCN3.4 can be confirmed by the temperature ramp test in the melt state at a constant dynamic mechanical condition and linear stress relaxation test. For two polymers having the same average molar mass but different molar mass distribution (MMD), the vertical shift of this cross-over point towards a low G-value indicates a wider MMD; where as, for two polymers having the same MMD but different average molar mass, the horizontal shift of this cross-over point towards the low frequency region indicates high average molar mass.[30] From Figure 3, we can see that the crossover point between G' and G'' shifts in both vertical and horizontal directions, which indicates that the polymer and the nanocomposites have different average molar mass with different MMDs. Both moduli of pure LCP systematically increase with increase in clay loading (see Figure 4). Such a result is expected because the incorporation of layered silicate particles induces some stiffness in the matrix polymer.

To explain these unusual frequency sweep results, SWAXS analysis of pure LCP and nanocomposite samples were carried out at 280 °C. Parts a–c of Figure 5 shows the 2-D SWAXS pattern of LCP, LCPCN1.4 and LCPCN3.4 samples at 280 °C. The SWAXS pattern at 280 °C shows the presence of a huge number of unaligned crystals of LCP
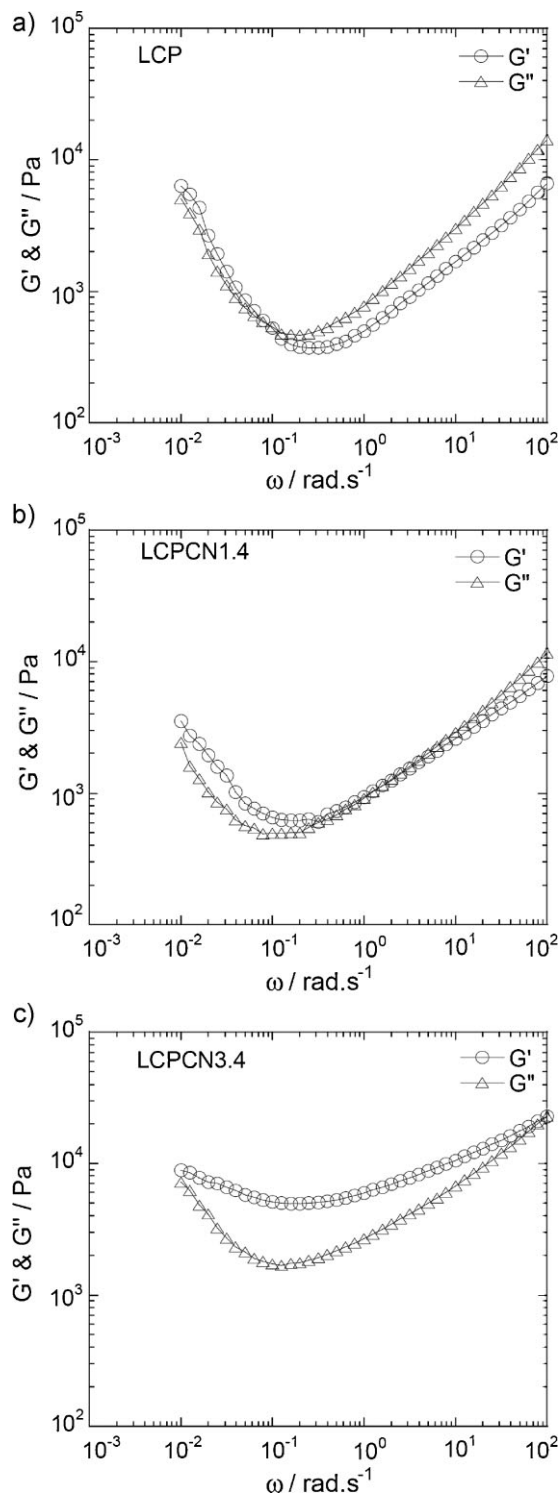

Figure 3. Frequency dependence of storage modulus (G') and loss modulus (G'') of (a) LCP, (b) LCPCN1.4 and (c) LCPCN3.4 measured at strain = 1% and temperature = 290 °C under nitrogen atmosphere.
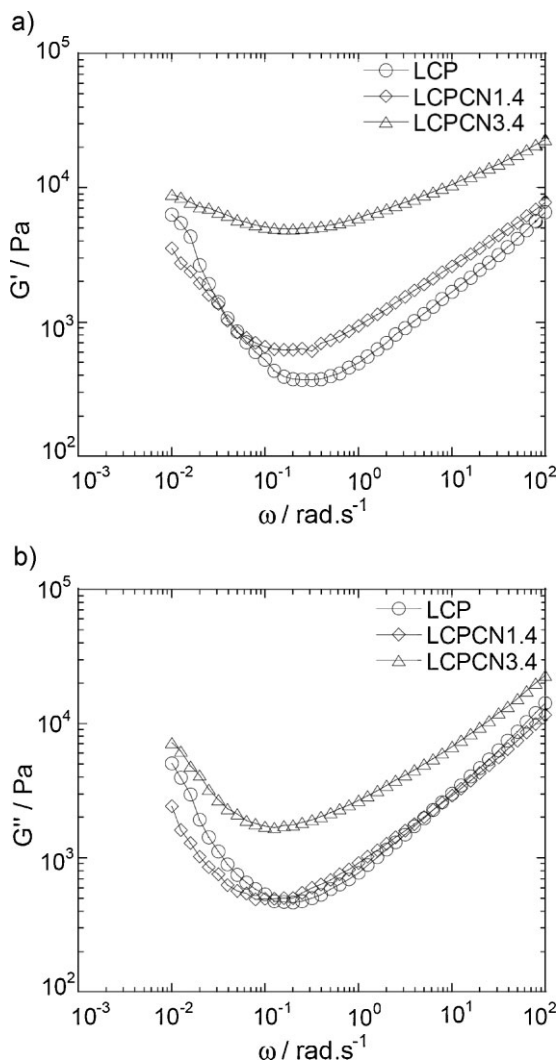
a)

b)

Figure 4. Effect of addition of C20A on the storage (G') and loss (G'') moduli of LCP measured at strain = 1% and temperature = 290 °C under nitrogen atmosphere.

Figure 5. 2-D SWAXS-patterns of (a) LCP, (b) LCPCN1.4 and (c) LCPCN3.4 at 280 °C.

There is a suppression of crystallinity in nanocomposites; however, there are still some unaligned crystals present (see Figure 5b and c). Under shear force they try to orient themselves in order to attain ordered structure. Since the amount of unaligned crystals decreases (Figure 5) with increase in organoclay content, the uplifting nature of the plots (Figure 4) decreases with increase in clay content. Similarly, uplifting point moves towards low frequency region as clay content increases. Details regarding SWAXS analyses can be found in our forthcoming article.[32]

The frequency dependence of complex viscosity, $|\eta*|$ of pure LCP matrix, and its nanocomposite samples are

in the wide-angle region compared to the nanocomposite samples. During frequency sweep experiments, at the beginning, the higher oscillation frequency cannot make a significant change in the alignment or ordering of those crystals. So because of less ordering they are easy to flow and this makes LCP less viscous. After a certain time and at very low frequencies where it can be assumed that the sample is almost at rest, the polymer crystallites get enough time to orient or to attain a smectic-like phase or more ordered structure.[31] Consequently, the elastic behaviour is dominant over the viscous behaviour ($G' > G''$) in the very low frequency region. On the other hand, in the case of nanocomposites (Figure 5b and c), the confinement of polymer chains in the well-ordered galleries of organoclay results the reduction in polymer's liquid crystallinity (see wide angle region in 2-D SWAXS patterns) with increase in clay loading.
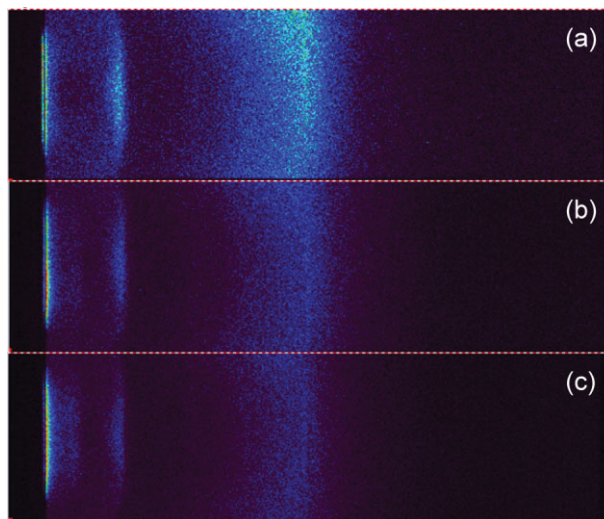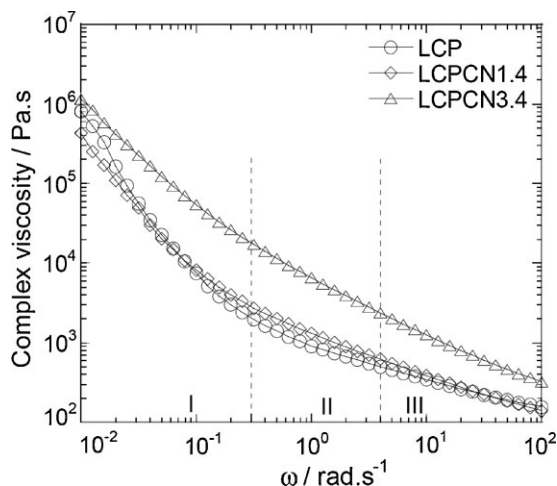

Figure 6. Frequency dependence of complex viscosity of neat LCP and nanocomposite samples measured at strain = 1% and temperature = 290 °C under nitrogen atmosphere.

presented in Figure 6. According to the result, LCP shows three regions: a shear thinning region (region I) in the low frequency range, another shear thinning region at the high frequency (region III), and a small plateau region between the two (region II). In the high frequency region (region III) one can imagine that the relative motion between the entangled structures is limited and hence most of the molecules are immobilised or conceptually in the frozen state. Therefore, the maximum part of the deformation energy can be stored here. In other words, in region III, the amount of deformation energy lost by friction between the molecules due to the relative motion is reduced, resulting in a decrease in $|\eta*|$. As the frequency decreases, the smaller molecules start to flow, and as a result, viscosity increases; but it is still difficult for the longer molecules to glide along each other, and hence, their entanglements start to form a temporary network. For this reason, the elastic property increases slightly and a nearly plateau region (region II) appears. After that, viscosity increases again as ω decreases (region I) and tries to attain zero shear viscosity (η_o) value since $\eta_o = \lim_{\omega \to 0} |\eta*(\omega)|$. Like pure LCP matrix, LCPCN1.4 also shows the three regions in the viscosity curve; however, region II is steeper compared to pure LCP. On the other hand, LCPCN3.4 shows only the shear-thinning behaviour. This is quite natural because the dispersed clay layers restrict the movement of polymer chains, and hence the sample shows more inflexibility and rigidity.

Temperature Sweep Test

Liquid-crystal polymer generally shows crystallinity in the melt state. To understand the effect of temperature on the change in liquid crystalline phases or the formation of network-like structures, the temperature sweep experiment of pure LCP and two different nanocomposite samples were conducted. In this type of oscillatory test, both the frequency and the strain amplitude are kept constant in each test interval; the only variable parameter is temperature. Parts a–c of Figure 7 shows the variation of G', G'' and tan δ of pure LCP and nanocomposite samples as a function of temperature upon heating from 290 to 350 °C with a ramp rate of 5 °C · min^{-1} at constant $\gamma = 1\%$ and $\omega = 6.283$ rad · s^{-1} under a nitrogen environment. It is clear from figures, for all samples, both moduli (G' and G'') initially start to decrease with temperature up to $\sim$305 °C. However, in case of LCPCN1.4 the initial drops of both moduli are sharp than that of LCP. Such an observation is very obvious because LCPCN1.4 is at the gel point at this experimental condition. After 305 °C, for all samples, the G' curves attain almost a plateau, where as G'' curves still decaying exponentially. For better understanding, the results are summarised in Table 2. At 290 °C the viscous behaviour is more dominant in LCP than in LCPCN1.4;
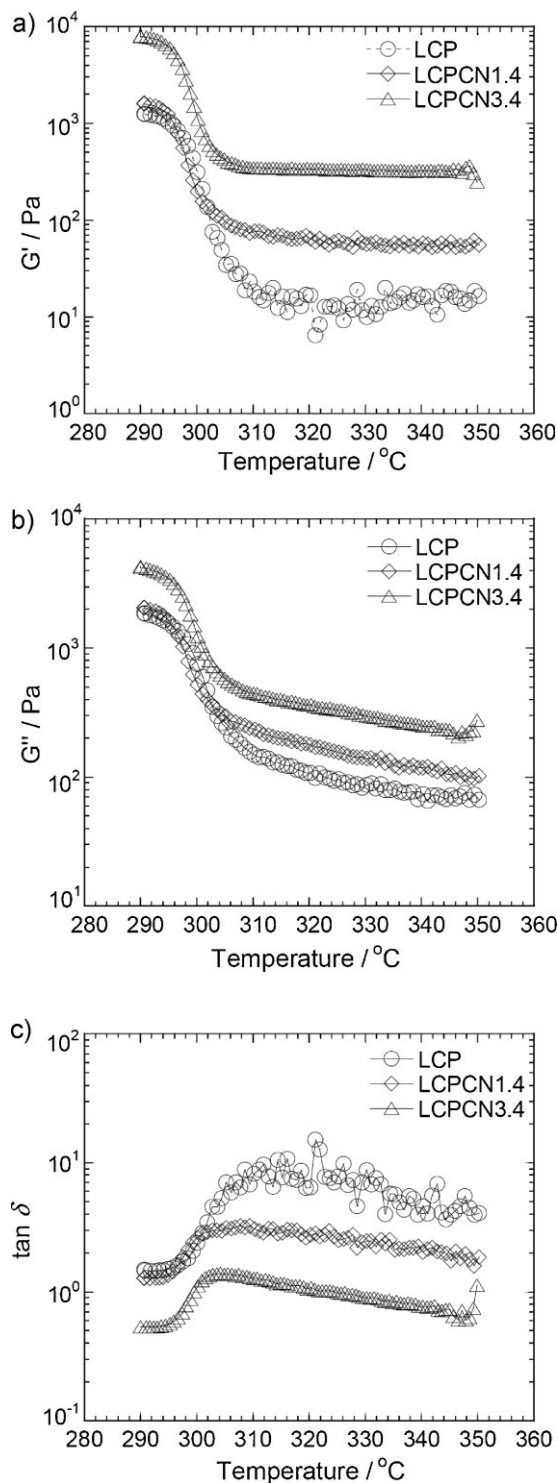

Figure 7. Temperature dependence of (a) storage modulus (G'), (b) loss modulus (G'') and (c) tan δ of pure LCP and nanocomposite samples at melt state. Frequency = 6.28 rad · s^{-1}, strain = 1% and temperature ramp rate = 5 °C · min^{-1}.

Table 2. Parameters determined from the temperature ramp test.

Sample	G'	G''	$T_{\tan\delta \text{ peak}}$
	Pa	Pa	°C
LCP	1 295	1 768	310
LCPCN1.4	1 642	2 065	302
LCPCN3.4	7 890	4 205	302

however, LCPCN3.4 shows elastic dominating behaviour ($G' > G''$) throughout the temperature range examined (Figure 7a and b). This means even at higher temperatures the material cannot reach a liquid state and exhibits a characteristics of a soft solid instead of a liquid melt. Moreover, the cross-linked or network-like structure is very stable in the case of LCPCN3.4. On the other hand, in a tan δ curve of LCP (Figure 7c), there is a transition (probably from a less ordered nematic-like to a more ordered smectic-like phase) around 310 °C, and this phenomenon becomes more prominent with the addition of layered silicate particles. In the case of the nanocomposite samples, this peak temperature systematically moves to the lower temperature as the clay loading increases (Table 2). Such an observation suggests that layered silicate particles have a strong effect on the change in director orientation or the change from a nematic-like to a smectic-like phase, which

is responsible for the enhanced pseudosolid-like behaviour as observed in the case of LCPCN3.4. Again, since the onset temperature of this transition is around 292 °C, during the frequency sweep tests at 290 °C one can expect an increase in the ordering in the system in the lower-frequency regions, which is responsible for the observed enhancement of the G' value in the case of the pure LCP and nanocomposite samples (see Figure 3). The above explanations and conclusions are supported by the SAXS patterns and DSC results as described in follow up article.[32]

Stress Relaxation Behaviour

To verify the unusual rheological properties of LCP upon nanocomposite formation, linear stress relaxation measurements of pure LCP and nanocomposite samples were carried out. Figure 8 shows the results of the linear stress relaxation behaviours of various samples at 290 °C during the imposition of 1% strain for 500 s. Although the strain step is not instantaneous, the samples experience a shock-like strain jump. As a result, the shapes of the super structures are deformed and internal stresses in the samples increase. As a result the stress (τ)-curves show a yield peak initially (see Figure 8b), after which, the samples try to return to the stress-free rest state where the super structures relax more and more from the forced strain by reducing the internal stress slowly, compensating for the motion within the super structures. At the end of the test, the molecules come back to the initial state of rest.

According to the Maxwell model,[30] a viscoelastic material can be considered as a summation of a series of combinations of a spring and a dashpot. For a single element—i.e. one spring (of elastic modulus, G and strain, γ_1) and a dashpot (of viscosity, η and strain, γ_2)—the Maxwell model can be represented as

$$\gamma = \gamma_1 + \gamma_2 \tag{1}$$

and therefore,

$$\tau(t) = \int_{-\alpha}^{t} \left[\frac{\eta}{\lambda} e^{(t-t')/\lambda}\right] \dot{\gamma}(t') \mathrm{d}t' \tag{2}$$

where the relaxation time (λ)

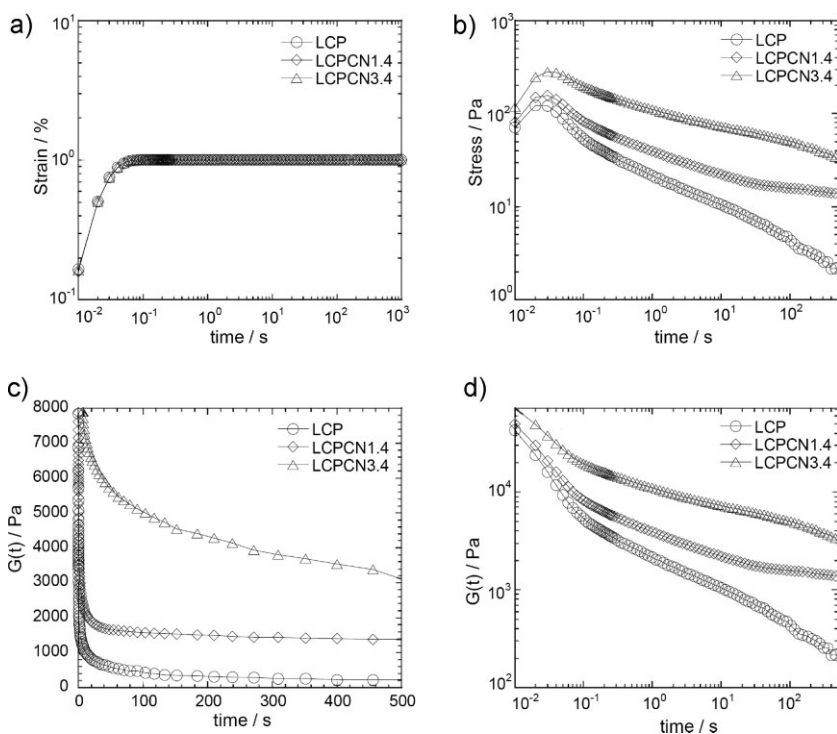$$\lambda = \eta/G \tag{3}$$

Figure 8. Stress relaxation behaviour of LCP and LCPCNs at 290 °C under nitrogen atmosphere: (a) applied step strain, (b) stress relaxation curves, (c) relaxation modulus curves presented on a linear scale and (d) relaxation spectra.

and relaxation modulus [$G(t)$],

$$G(t) = \frac{\eta}{\lambda} e^{-(t-t')/\lambda} \qquad (4)$$

Now, at $t = 0$, $G(t)$ reduces to G_o, and hence, Equation (2) reduces to[30]

$$\tau(t) = G_0 e^{-(t/\lambda)} \gamma \qquad (5)$$

At time point $t = \lambda$ [30]

$$\tau(\lambda) = \gamma G_0 (1/e) = 0.368 \gamma G_0 = 36.8\% \gamma G_0$$
$$= 36.8\% \tau_{max} \qquad (6)$$

The relaxation time represented by Equation (3) reflects the speed with which the stress relaxes and not the interval of time within which the stress relaxes. Therefore, the lower relaxation time corresponds to a faster stress relaxation. To determine the relaxation time, first, $\tau(\lambda)$ was calculated according to Equation (6) and then λ was determined from Figure 8b. The results are tabulated in Table 3. According to the table, the value of λ follows the order LCPCN3.4 > LCPCN1.4 > LCP, which means the pure LCP matrix relaxes faster than nanocomposites.

Figure 8b shows the steeply falling nature of LCP when compared to LCPCNs, while LCP is showing a relaxation behaviour which is close to the behaviour of a viscoelastic liquid and LCPCN1.4 shows τ-curve approaching an equilibrium value, τ_e. These results support the behaviour of a partial relaxation like viscoelastic solids, as we observed during frequency sweep tests. On the other hand, LCPCN3.4 shows less relaxation ability compared to LCPCN1.4. Since a viscoelastic solid material consists of a partial chemical or physical network (partial cross-linking), one can conclude that the cross-linking increases with the clay loading.

Figure 8c and d show how the relaxation modulus, $G(t)$ changes with time. For LCP, $G(t)$ falls very rapidly and attains an equilibrium value G_e much more quickly than for the nanocomposite samples, suggesting that it is very easy to orient pure polymer chains in the flow direction. However, for nanocomposite samples, especially with

Table 3. Determination of relaxation time.

Sample	λ
	s
LCP	0.15
LCPCN1.4	0.32
LCPCN3.4	2.35

higher clay content, the structures are more stable. This observation actually supports the previous conclusions.

Rotational Tests

The purpose of the following rotational tests is to observe the structure regeneration ability after the destruction of the original structure of the material.

Step Rate Test

The step rate test was performed in order to determine the amount of recovery of the structure after breaking the internal structure. This test consists of four successive steps as shown in Figure 9a. In the first step, a very low shear rate ($\dot{\gamma} = 0.01$ s^{-1}) was applied for 1 000 s, and the
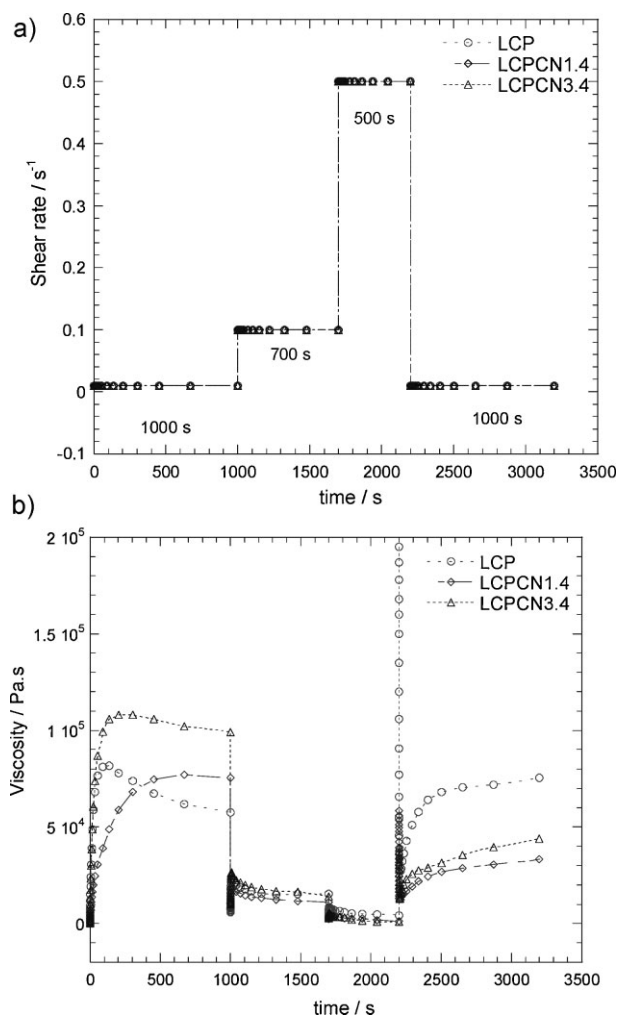

Figure 9. (a) Stepwise variation of shear rate with time and (b) the corresponding change in viscosity. Measuring temperature = 290 °C under nitrogen and frequency = 6.28 rad · s^{-1}.

Table 4. Determination of structure present after destruction and regeneration.

	LCP		LCPCN1.4		LCPCN3.4	
	η	Regeneration	η	Regeneration	η	Regeneration
	Pa	%	Pa	%	Pa	%
At the end of the first interval (reference η value)	81 865	100	75 498	100	107 331	100
At the end of the second interval	16 077	20	11 125	15	13 247	12
At the end of the third interval	4 758	6	514	0.7	514	0.5
Regeneration in the forth interval						
After 300 s	67 717	83	25 273	33	30 932	29
After 600 s	71 961	88	29 517	39	38 006	35
After 1 000 s	75 498	92	32 347	43	42 250	39

change in viscosity with time was recorded (Figure 9b). From the figures, it is clear that the LCPCNs are showing fairly constant η value, but pure LCP is showing a shear thinning nature. Generally, LCP shows three regions in the flow curve: first a shear thinning region (region I), next a plateau (region II) and finally, another shear thinning region (region III).[33–38] To explain this behaviour, Marrucci and Maffettone suggested that the LCP system can be viewed as a suspension of defects in the nematic phase. With increase in the shear rate, the progressive modification in the defect structure results in a decrease in contribution of defects to the viscosity; hence, a shear thinning region (region I) appears. The defects act as internal anchoring walls for the directors of the tumbling nematic. A system constituting defect cores is less ordered than the nematic phase and would not tumble. Thus, with increase in shear rate, when the contribution of defects becomes negligible, a dynamic equilibrium reaches for any assigned shear rate at an appropriate defect density. This actually corresponds to region II. After exceeding a certain shear rate, the tumbling behaviour of the directors' changes to a wagging motion, wherein the directors oscillate back and forth along the flow direction.[39] The frequency of the wagging motion increases with further increase in shear rate. This results in the second shear thinning region (region III). Therefore, it is clear that the initial shear thinning behaviour of pure LCP matrix is due to the modification of defect structures (region I, Figure 8b). On the other hand, nanocomposites have fewer defects due to the intercalated structure and, hence, show a plateau as compared to pure LCP. Anyway, the viscosity value at the end of this range will be used later as reference value in Table 4. Due to the sudden jump in shear rate ($\dot{\gamma} = 0.1$ s^{-1}), the structures of all the samples break down to a certain extent.

Because of this structural decomposition, the tumbling motion increases suddenly, and the samples show very low η value. Further increment of shear rate ($\dot{\gamma} = 0.5$ s^{-1}) results in almost complete structural decomposition. In the final shear zone, known as the regeneration interval, the same shear conditions like as in the first interval facilitate the regeneration of the samples structure. According to Table 4, the true regeneration values (regeneration after 1 000 s–the structure present after the third interval) are 86, 42.3 and 38.5%, for LCP, LCPCN1.4 and LCPCN3.4, respectively.

Step Rate Relaxation Tests

The purpose of this experiment was to see how a material reacts to an instantaneous change of flow. Initially, the samples were treated under 0.5 s^{-1} shear rates for 1 000 s at 290 °C and then allowed to relax for another 2 000 s as demonstrated in Figure 10. Although during the step rate test at the same shear rate all samples showed almost a plateau region, during this test they showed completely different behaviour. The sudden application of a high shear rate (compared to the shear rates applied initially during the step rate test) modifies the defects in the LCP very quickly and attains almost the equilibrium position (region II). On the other hand, nanocomposites show shear thinning behaviour, the region III behaviour which may be due to the wagging motion. According to the step rate test LCPCNs exhibit less shear thinning compared to the LCP in the first shearing zone. That means in this shear region when pure LCP shows region I behaviour, LCPCNs show region II behaviour. Therefore, it is possible for LCPCNs to attain region III much faster than pure LCP. For this reason, when the samples undergo relaxation, there is no defect present in the samples, and hence, they are almost relaxed.
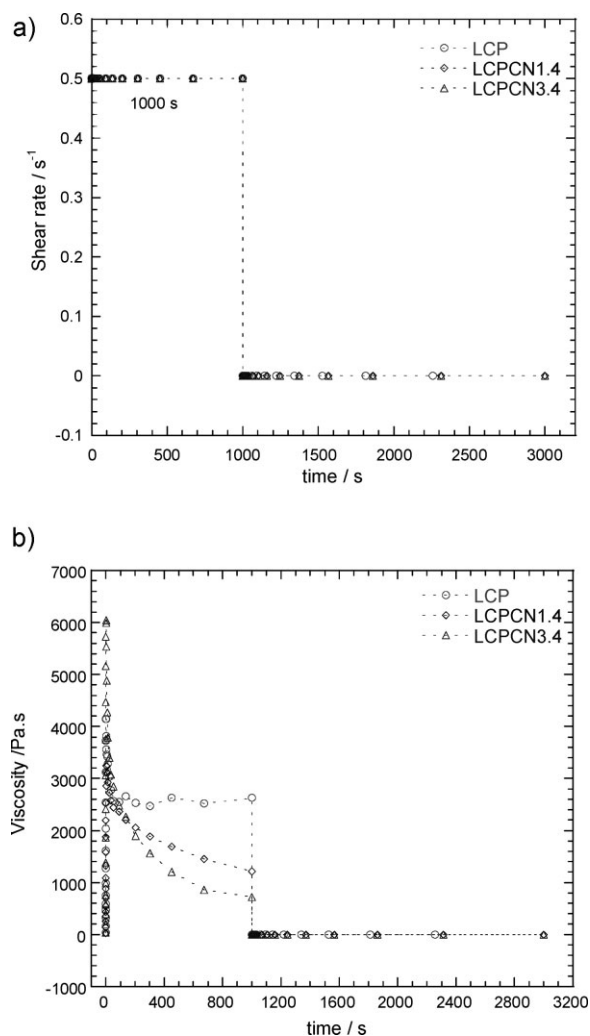
Figure 10. Variation of (a) shear rate and (b) viscosity during step rate relaxation test, measured at 290 °C under nitrogen atmosphere and frequency $= 6.28$ rad · s^{-1}.

explain such phenomena very nicely. Since the amount of unaligned crystal decreases with increase in clay loading, the shear induced alignment phenomena in the low frequency region becomes less pronounced with increase in clay content.

According to the temperature sweep test results, the viscous behaviour is more dominant in LCP compared to LCPCN1.4; however, LCPCN3.4 shows $G' > G''$ throughout the temperature range examined, since it possesses more cross-linked structures. The relaxation ability of LCP reduces after intercalation of polymer chains into the two-dimensional silicate galleries.

The step rate test was performed in order to determine the amount of recovery of the structure after breaking the internal structure. In the regeneration interval, LCP, LCPCN1.4 and LCPCN3.4 can recover 86, 42.3, and 38.5% of the original structure, respectively. During the step rate relaxation test, high shear rate modifies the defects in the LCP very quickly and attains almost the equilibrium position. The nanocomposites show shear thinning behaviour because of the wagging motion. So, when the samples undergo relaxation, there is no defect present in the samples, and hence, they are almost relaxed. In our forthcoming article, most of our conclusions will be supported by SWAXS and deferential scanning calorimeter studies.

Conclusion

In conclusion, this article summarises the melt-state rheological property of LCP and how it changes in the presence of organoclay. LCP and LCPCN3.4 show the formation of gel structure, in the LVE region. Even if this is a weak gel structure, the samples exhibit a certain form-stability. On the other hand, LCPCN1.4 shows 'at the gel point' behaviour, where the material is at the borderline between gel (solid) and sol (liquid) structures under the same experimental conditions. Such a result indicates, at this particular frequency of oscillation, the structure of LCPCN1.4 is more flexible than LCPCN3.4 and pure LCP.

For all samples, the frequency sweep results show some unusual behaviour (uplifting nature of both G' and G'') in the low frequency region. The 2-D SWAXS patterns can

[1] K. I. Winey, R. A. Vaia, *MRS Bull.* **2007**, *32*, 314.
[2] S. Sinha Ray, M. Okamoto, *Prog. Polym. Sci.* **2003**, *28*, 1539.
[3] S. Sinha Ray, M. Bousmina, *Prog. Mater. Sci.* **2005**, *50*, 962.
[4] M. Alexandre, P. Dubois, *Mater. Sci. Eng. R.* **2000**, *28*, 1.
[5] F. F. Fang, H. J. Choi, J. Joo, *J. Nanosci. Nanotechnol.* **2008**, *8*, 1559.
[6] J. Zhang, E. Manias, C. A. Wilkie, *J. Nanosci. Nanotechnol.* **2008**, *8*, 1597.
[7] I. S. Gunes, S. C. Jana, *J. Nanosci. Nanotechnol.* **2008**, *8*, 1616.
[8] D. R. Paul, *Polymer* **2008**, *49*, 3187.
[9] R. Valsecchi, M. Vigno, M. Levi, S. Turri, *J. Nanosci. Nanotechnol.* **2008**, *8*, 1835.
[10] V. Causin, C. Marega, A. Marigo, G. Ferrara, A. Ferraro, R. Selleri, *J. Nanosci. Nanotechnol.* **2008**, *8*, 1823.
[11] K. M. Lee, C. D. Han, *Polymer* **2003**, *44*, 4573.
[12] P. C. Lebaron, Z. Wang, T. J. Pinnavaia, *Appl. Clay Sci.* **1999**, *15*, 11.
[13] J. X. Lee, J. Wu, C. M. Chan, *Polymer* **2000**, *41*, 6935.
[14] R. A. Vaia, E. P. Giannelis, *Polymer* **2001**, *42*, 1281.
[15] J. H. Chang, B. S. Seo, D. H. Hwang, *Polymer* **2002**, *43*, 2969.
[16] G. Zhang, C. Jiang, C. Su, *J. Appl. Polym. Sci.* **2003**, *89*, 3155.

[17] W. Huang, C. D. Han, *Macromolecules* **2006**, *39*, 257.
[18] W. Huang, C. D. Han, *Polymer* **2006**, *47*, 4400.
[19] M. M. Shen, M. G. Lu, Y. L. Chen, C. Y. Ha, *Polym. Int.* **2005**, *54*, 1163.
[20] J. H. Chang, C. H. Ju, S. H. Kim, *J. Polym. Sci. Part B Polym. Phys.* **2006**, *44*, 387.
[21] T. S. Chung, M. Cheng, P. K. Pallathadka, S. H. Goh, *Polym. Eng. Sci.* **1999**, *39*, 953.
[22] X. Hu, Q. Lin, A. F. Yee, D. Lu, *J. Microsc.* **1997**, *185*, 109.
[23] J. Bandyopadhyay, S. S. Ray, M. Bousmina, *Macromol. Chem. Phys.* **2007**, *208*, 1979.
[24] D. Shi, Z. Ke, J. Yang, Y. Gao, J. Wu, J. Yin, *Macromolecules* **2002**, *35*, 8005.
[25] H. S. Jeon, A. I. Nakatani, C. C. Han, *Macromolecules* **2000**, *33*, 9732.
[26] M. Kapnistos, A. Hinriches, D. Vlassopoulos, S. H. Anastasia-dis, A. Stammer, B. A. Wolf, *Macromolecules* **1996**, *29*, 7155.
[27] I. S. Polios, M. Soliman, C. Lee, S. P. Gido, K. Schmidt-Rohr, H. H. Winter, *Macromolecules* **1997**, *30*, 4470.
[28] S. Sinha Ray, *J. Ind. Eng. Chem.* **2006**, *12*, 811.
[29] P. Cassagnau, *Polymer* **2008**, *49*, 2183.
[30] T. G. Mezger, *"The Rheology Handbook"*, 2nd edition, Vincentz, Germany 2006.
[31] H. A. Baghdadi, J. Parrella, S. R. Bhatia, *Rheol. Acta* **2008**, *47*, 349.
[32] J. Bandyopadhyay, S. Sinha Ray, M. Bousmina, *Polymer,* in press.
[33] R. G. Larson, *"The Structure and Rheology of Complex Fluids"*, Oxford University Press, New York 1999.
[34] C. Noel, P. Navard, *Prog. Polym. Sci.* **1991**, *16*, 55.
[35] G. Marrucci, *J. Phys. Condens. Matter* **1994**, *6*, A305.
[36] J. Mewis, M. Mortier, J. Vermantg, P. Moldenaers, *Macromol-ecules* **1997**, *30*, 1323.
[37] W. J. Zhou, J. A. Kornfield, W. R. Burghardt, *Macromolecules* **2001**, *34*, 3654.
[38] N. Grizzuti, S. Cavella, P. Cicarelli, *J. Rheol.* **1990**, *34*, 1293.
[39] R. G. Larson, *Macromolecules* **1990**, *23*, 3983.